

Stochastic Growth Dynamics and Composite Defects in Quenched Immiscible Binary Condensates

I.-K. Liu,^{1,2} R. W. Pattinson,² T. P. Billam,³ S. A. Gardiner,³ S. L. Cornish,³
T.-M. Huang,⁴ W.-W. Lin,⁵ S.-C. Gou,¹ N. G. Parker,² and N. P. Proukakis²

¹Department of Physics, National Changhua University of Education, Changhua 50058, Taiwan

²Joint Quantum Centre (JQC) Durham–Newcastle, School of Mathematics and Statistics,
Newcastle University, Newcastle upon Tyne, NE1 7RU, United Kingdom

³Joint Quantum Centre (JQC) Durham–Newcastle, Department of Physics, Durham University,
Durham, DH1 3LE, United Kingdom

⁴Department of Mathematics, National Taiwan Normal University, Taipei 11677, Taiwan

⁵Department of Applied Mathematics and Shing-Tung Yau Center,
National Chiao Tung University, Hsinchu 30010, Taiwan

We study the sensitivity of coupled condensate formation dynamics on the history of initial stochastic domain formation in the context of instantaneously quenched elongated harmonically-trapped immiscible two-component atomic Bose gases. The spontaneous generation of defects in the fastest condensing component, and subsequent coarse-graining dynamics, can lead to a deep oscillating microtrap into which the other component condenses, thereby establishing a long-lived composite defect in the form of a dark-bright solitary wave. We numerically map out diverse key aspects of these competing growth dynamics, focussing on the role of shot-to-shot fluctuations and global parameter changes (initial state choices, quench parameters and condensate growth rates). We conclude that phase-separated structures observable on experimental timescales are likely to be metastable states whose form is influenced by the stability and dynamics of the spontaneously-emerging dark-bright solitary wave.

PACS numbers: 03.75.Mn, 03.75.Lm, 03.75.Kk

Introduction: Pattern formation and the presence of coexisting phases in spatially separated domains are an emergent feature of diverse dynamical systems throughout physics [1], chemistry [2], and biology [3]. Ultracold gases offer a highly controllable theoretical and experimental test-bed for studying these phenomena, particularly in the context of condensate formation dynamics [4–6], a subject of sustained interest and significance in non-equilibrium physics, both in the ultracold gas context [7–20], and beyond [21–24]. Previous works have highlighted the generic importance of the Kibble-Zurek (KZ) mechanism in defect formation during phase transitions [25, 26], connecting ultracold gases with a range of phenomena from high-energy and condensed matter physics [27–29], with composite defects [30] emerging in the context of multi-component fields by condensation in the defect core [31].

Experiments with single-component atomic Bose-Einstein condensates (BECs) have revealed the spontaneous formation of defects in the form of vortices [32], dark solitonic vortices [33, 34] and persistent currents [35] during the BEC phase transition, providing quantitative confirmation of KZ scaling [19, 36–39]. In multi-component BECs (e.g. ^{87}Rb - ^{41}K [40], ^{87}Rb - ^{85}Rb [41] and ^{87}Rb - ^{133}Cs [42, 43]), studies of KZ effects have focused on the formation of two same-species BECs in a tunnel-coupled geometry [44], and quantum phase transitions in binary [45–47] and spinor Bose gases [39, 48–53]. Work on homogeneous spinor Bose gases [50, 51] has identified two distinct timescales in the process of domain formation: a short timescale for initial domain formation via the KZ mechanism, and a long “memory” timescale for nonlinear coarse-graining dynamics to erase traces of the initial domains. Related work indicates that characteristic memory timescales may exceed experimental system lifetimes [52, 53].

In this Rapid Communication we discuss the competing growth dynamics of instantaneously-quenched immiscible two-component BECs, providing strong evidence that the density profiles emerging over experimentally relevant timescales are determined by the history of spontaneous defect formation, and subsequent dynamics [Fig. 1]. This long-term memory is facilitated by the added stability provided by the formation, during coarse-graining dynamics, of a composite dark-bright solitary wave [54–59] defect, a process found to be robust to perturbations, but sensitive to shot-to-shot fluctuations and global parameter changes.

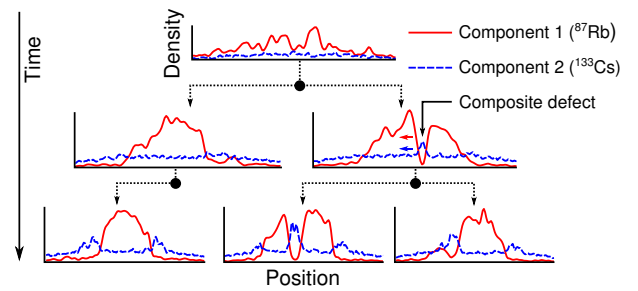


FIG. 1. (color online). Memory of stochastic defect dynamics in an immiscible two-component condensate (schematic, compiled from simulation data). On short post-quench time scales, the fastest-condensing component (here ^{87}Rb) contains multiple spontaneously-generated defects (top). The ensuing stochastic dynamics generically lead to either destruction of defects, or survival of a single composite defect in which the second component (here ^{133}Cs) preferentially condenses, forming a dark-bright solitary wave (middle row). The long-lived metastable states corresponding to experimental observations (bottom row) retain a memory of the prior stochastic dynamics.

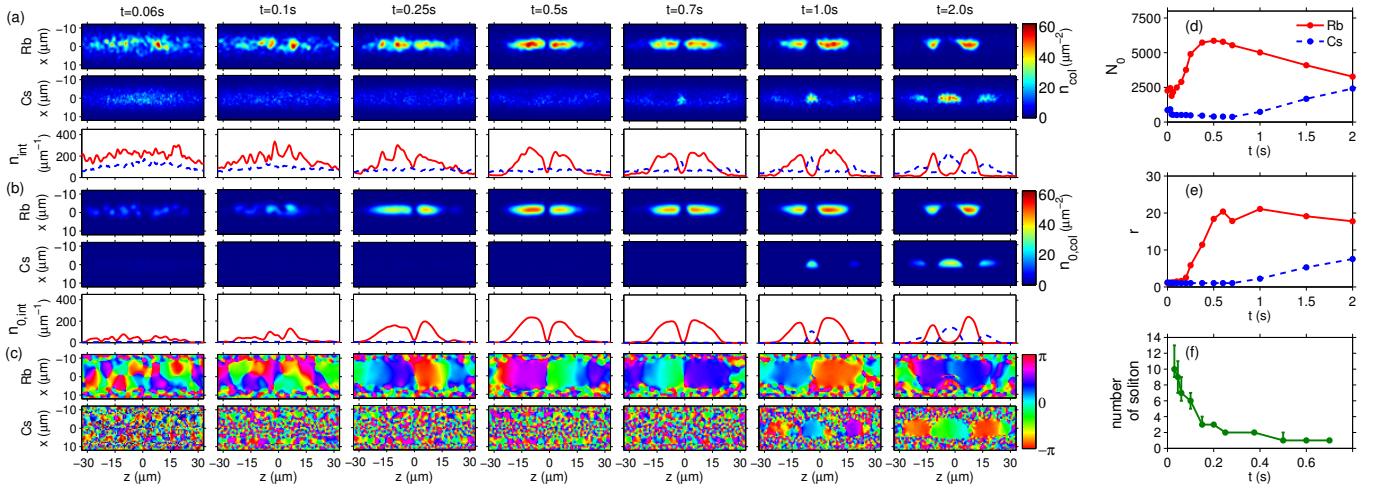


FIG. 2. (color online) Typical numerical evolution of a quenched two-component system. (a)–(b) show post-quench evolution, up to 2 s, of 2D column densities (n_{col} , $n_{0,\text{col}}$) and 1D integrated density profiles (n_{int} , $n_{0,\text{int}}$) for c-field and Penrose-Onsager condensate respectively, while (c) shows the corresponding condensate phase. (d)–(e) show the evolution of (respectively) the condensate number, N_0 , and the occupation ratio, r , between the condensate mode and the next-most-highly occupied mode, with (f) showing the evolution of the number of spontaneously-generated dark solitons resulting from the quench (obtained by looking at density minima and phase jumps, similar to the procedure of [37]). In all simulations in this work, both components are confined in harmonic traps with frequencies ($\omega_z^{\text{Rb}}, \omega_{\perp}^{\text{Rb}}, \omega_z^{\text{Cs}}, \omega_{\perp}^{\text{Cs}}$) = $2\pi \times (3.89, 32.2, 4.55, 40.2)$ Hz, with longitudinal and transverse shifts of ~ 1 μm in their centers [42, 60], and scattering lengths ($a_{\text{Rb,Rb}}, a_{\text{Cs,Cs}}, a_{\text{Rb,Cs}}$) = $(100, 280, 650) \times a_0$ (a_0 : Bohr radius). Initial states are at a temperature $T_0 = 80$ nK, approximately equal to the corresponding ideal gas critical temperature T_c , and the instantaneous quench reduces this to $T = 20$ nK. In the first part of this work, we use initial chemical potentials $\mu_{\text{Rb}}/k_{\text{B}} = 2.13$ nK, $\mu_{\text{Cs}} = 0.956\mu_{\text{Rb}}$ ($\mu_{\text{Rb}} = 1.38\hbar\omega_{\perp}^{\text{Rb}}$, $\mu_{\text{Cs}} = 1.05\hbar\omega_{\perp}^{\text{Cs}}$), and rates $\gamma_{\text{Rb}} = \gamma_{\text{Cs}} = 0.263$ s $^{-1}$ (equivalent to $\hbar\gamma_{\text{k}}/k_{\text{B}}T = 10^{-4}$), with $\mu'_{\text{Rb}} = \mu_{\text{Rb}}$, $\mu'_{\text{Cs}} = 7.34\mu_{\text{Cs}}$. The initial condition is an equilibrated state with few macroscopically occupied modes, but no definite condensate mode, $r \sim 1$.

While the equilibrium states of immiscible two-component BECs in the mean-field approximation are known to display various symmetric and asymmetric structures [60, 61] similar to those observed in experiment [41, 42], in this work we show similar structures emerging as part of a rich non-equilibrium dynamical behavior long *before* the system has reached an equilibrium state. Our work yields insight into the complexities of two-component BEC formation, and indicates caution when concluding that an experimental immiscible two-component BEC has reached a true equilibrium state.

Quench Protocol and Modeling Details: Our analysis is based on a sudden temperature and chemical potential quench of a prolate (aspect ratio ≈ 10) two-component atomic cloud of approximately 1.4×10^6 ^{87}Rb and 8×10^5 ^{133}Cs atoms, equilibrated in slightly displaced traps at $T_0 = 80$ nK (further details in the caption of Fig. 2), approximately equal to the corresponding ideal gas critical temperature T_c . Based on a characteristic example (Fig. 2), in which neither component initially possesses a single macroscopically-occupied mode, we analyze the role of fluctuations and quench parameters [Figs. 3, 4(a)], under the assumption that Rb condenses fastest. Analyzing this scenario for a variety of initial states and quenches, we critically discuss the main assumptions [Figs. 4(b)–5], thus providing, within current computational constraints, a qualitative characterisation of the dynamical phase diagram..

Dynamical two-component BEC simulations to date have been based on coupled ordinary [54, 55, 62, 63] or dissipative

[20, 64, 65] Gross-Pitaevskii equations (GPEs), classical field [66], truncated Wigner [45, 46], or ZNG (coupled GPE-Boltzmann) [67] methods. The effects of thermal fluctuations during condensate growth are best captured by 3D coupled stochastic projected Gross-Pitaevskii equations [53, 68, 69],

$$d\psi_k = \mathcal{P} \left\{ -\frac{i}{\hbar} L_k \psi_k + \frac{\gamma_k}{k_{\text{B}} T} (\mu_k - L_k) \psi_k \right\} dt + dW_k, \quad (1)$$

describing the evolution of highly-occupied “classical” modes ψ_k , where k labels the species (here Rb or Cs). Here $L_k = -\hbar^2 \nabla^2 / 2m_k + V_k + 4\pi\hbar^2 (a_{kk} |\psi_k|^2 / m_k + a_{kj} |\psi_j|^2 / M_{kj})$, for scattering lengths a_{kk} (intraspecies) and a_{kj} (interspecies), atomic masses m_k , and reduced mass M_{kj} . The “c-field” region defined by projector \mathcal{P} , consists of single-particle modes ϕ_l with energies below a carefully-selected energy cutoff [70], which is coupled to the above-cutoff reservoir at temperature T via growth (described by the species-dependent rates γ_k) and noise (described by dW_k [71]) processes. To simulate two-component condensate formation, we first obtain an equilibrated initial state by numerically propagating Eq. (1) to equilibrium for initial chemical potentials μ_k and common temperature $T_0 \gtrapprox T_c$, and then instantaneously quench these parameters to final values $T < T_c$ and $\mu'_k \geq \mu_k$. We extract the time-dependent condensate mode using the Penrose–Onsager (PO) criterion [72], by seeking a macroscopically-occupied eigenmode of the one-body density matrix in short-time averages over single trajectories [68].

Typical Coupled Dynamics Simulation: A typical numerical run of the post-quench dynamics demonstrating the formation of a composite defect for a given initial state ($\mu_k > 0$) and quench parameters (see figure caption) is shown in Fig. 2, a result with which subsequent ones will be compared. Snapshots (left panels) of the c-field density (a), condensate mode density (b), and condensate phase (c) reveal three characteristic evolutionary stages: (i) immediately after the quench, we observe a short “condensation onset” time with strongly non-equilibrium dynamics (for $\lesssim 0.1$ s) in which multiple quench-induced defects proliferate; (ii) this is followed by a rapid relaxation interval (here $t \lesssim 0.5$ s, featuring rapid Rb growth), largely characterised by defect coarse-graining dynamics, which leads to a metastable equilibrium state with a fixed number of long-lived defects; this number can be zero, one — as is the case here — or potentially higher; (iii) finally, a slow evolution towards a global equilibrium follows, in which the other component (here Cs) may (but need not) also condense. While the details of the coupled dynamics are, unsurprisingly, sensitive to global system and quench parameters, our subsequent analysis confirms that the occurrence of these three characteristic stages is generic. Within our model, for a given set of quench parameters, the long-term evolution tends to favor the dominance of *either* Rb or Cs.

The right panels in Fig. 2 show the dynamics of the (Penrose-Onsager) condensate atom numbers, N_0 , (d), the occupation ratio, r , of the condensate mode to the next-most-highly occupied mode (e), and the evolution of the number of observable defects [solitons, (f)]. They show that (i) while the initial state has no single macroscopically-occupied mode ($r \sim 1$), such a mode emerges dynamically (rapid increase of r) following the quench; (ii) coherence growth, caused by the suppression of phase fluctuations during condensation [15, 16], coincides with the rapid decrease in the defect numbers due to merging/decay [34]; (iii) due to the larger initial Rb atom number, Cs condensation sets in after the corresponding Rb process [41]; moreover, as our simulations do not include evaporative cooling, we find that Cs condensation is associated with a gradual decrease in the Rb condensate.

General considerations [29] suggest that, dependent on dimensionality, the nature of the emerging defect could also be a solitonic vortex, or vortex [73], whose infilling would create a (solitonic) vortex–bright soliton [74] rather than a dark–bright soliton. However, we observe defects when the geometry and parameters are such that $\mu'_{\text{Rb}} < 4\hbar\omega_{\perp}^{\text{Rb}}$ and $\mu_{\text{Cs}} < 8\hbar\omega_{\perp}^{\text{Cs}}$, favoring 1D solitonic defects [73].

In Fig. 2, the initial multiple defects in the fastest condensing component eventually lead to exactly one *long-lived* defect, which acts as a tight mobile microtrap [75], facilitating rapid condensation of the other component. Growth of the bright (infilling) component in the microtrap (which stabilizes the dark soliton against decay [64]) leads to a spontaneously-generated dark–bright soliton; for the particular simulation here, this soliton forms close to the trap centre. Over longer timescales, the growing mean-field potential converts this dark–bright solitary wave into a fixed domain wall [76, 77].

Subsequently, a Cs condensate also gradually appears at the edges of the system, slightly compressing the Rb condensate towards the trap center.

This interplay between condensate growth, defect formation and dissipative evolution in the first component, and condensate growth of the second component — alongside increasing mean-field repulsion between the co-forming immiscible condensates — leads to interesting features which should be observable in current experiments. To characterise these, we consider: (i) the role of shot-to-shot fluctuations (Fig. 3); (ii) the dependence on growth rates and final quench parameters when starting from quasi-condensate initial states (Fig. 4); and (iii) the changes to the evolution imposed by less coherent pre-quench states (Fig. 5). Importantly, we find that the scenario of a defect in Rb leading to Cs infilling, can be effectively reversed for appropriate parameter choice and timescales.

Shot-to-Shot Variations: We investigate sensitivity to fluctuations by looking at different numerical runs (loosely corresponding to different experimental runs) for the same fixed quench sequence [Fig. 3(a)–(d)]; such runs feature statistically-identical condensate number evolution [see error bars in Fig. 4(a)]. The “reference” case of Fig. 2 is shown in Fig. 3(a), revealing the evolutionary stages of slow-moving solitonic defect, near-stationary dark–bright solitary wave, and eventual static domain wall structure. Figures 3(b)–(d) reveal alternative (and roughly equally-likely) outcomes for different post-quench dynamical noise realizations (of the same mean amplitude), describing thermal fluctuations. Figure 3(c) shows slower Cs growth in an initially shallower, and hence

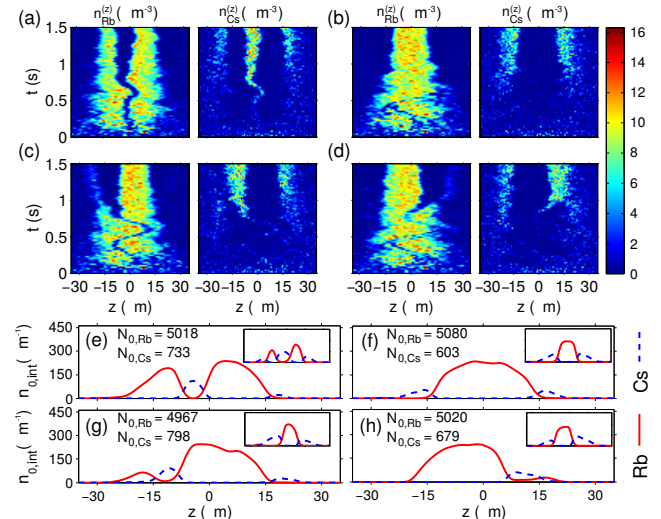


FIG. 3. (color online). Evolution for four different post-quench random noise sequences, with identical pre-quench state. (a–d) show the c-field density evolution [shown here via $n_k^{(z)} = n_k(x = 0, y = 0, z)$], and (e–h) the condensate density profiles after 1 s (insets 2 s). After this time the Rb defect has either: been stabilized by Cs infilling (e); fully decayed within Rb (f); or decayed to the left (g) or right (h) edge of the condensate. Quench parameters are as in Fig. 2.

more rapidly moving, dark solitary-wave microtrap. In contrast to Fig. 3(a), where dark solitary wave decay and stabilisation occurs at the trap center, Figs. 3(c)–(d) show dark solitary wave decay and stabilisation occurring either to the left (c), or to the right (d), illustrating the crucial role of the motion of the decaying dark solitary wave [78]. Figure 3(b) illustrates the potential for co-existence of more than one (shallow) defect for an appreciable time [see also Fig. 4(d) for $t \lesssim 0.5$ s], which typically decay without Cs growth in the solitonic microtraps; in such a case, Cs can only condense around Rb, where the mean-field repulsion is minimised. Figure 3(e)–(h) shows the condensate profile after 1 s (insets 2 s), consisting of either a large Cs structure in the middle separating the Rb [inset to (e)], or a large Rb structure enclosed by Cs [insets to (f), (g), (h)]. Further evolution of case (a) (to $\gtrsim 3$ s) also yields a near-centre Rb structure consistent with this scenario, after gradual merging of the two separated (decaying) Rb peaks.

While results presented so far were based on an identical initial state, but different post-quench dynamical noise, we have confirmed that our qualitative findings remain unchanged in identical simulations with different (random) thermalized initial states, as would be expected in different experimental runs. In particular, although different, randomly-generated, initial (pre-quench) states yield different post-quench defect formation dynamics, we find that at least 3 out of 9 simulations with both different initial and dynamical noise reveal clear evidence of spontaneous dark-bright soliton formation, with 2 of the emerging composite defects being relatively deep and central. Despite the differences in emergent density profile, condensate atom number evolution is the same [within statistical variations, see error bars in Fig. 4(a)], irrespective of the formation, stabilization or decay of the dark-bright solitary wave. The importance of dark-bright solitary waves in the early stages of formation is further confirmed through dissipative GPE simulations, showing that even perfectly-imprinted multiple dark-bright solitons quickly coalesce into a single long-lived dark-bright soliton, with rapid dynamical mean-field stabilisation.

Sensitivity to Trap Asymmetries: We find that the presence, or absence, of small asymmetries (~ 1 μm) in the trap minima only alter the details, but not the qualitative structure, of the emerging density profiles, indicating that fluctuations can strongly suppress experimentally relevant trap imperfections (whose role can dominate mean-field simulations [60]).

Dependence on Global Quench Parameters: Distinct regimes of coupled dynamical evolution arising for different quench parameters are shown in Fig. 4. We focus here on the dependence of N_0 on variations of the quench parameters (chemical potentials μ'_k , growth rates γ_k) for fixed initial quasi-condensate states. With $\gamma_{\text{Rb}} = \gamma_{\text{Cs}}$ held fixed, we find Rb dominates the evolution for a broad range of $\mu'_{\text{Rb}} > \mu_{\text{Rb}}$ [squares/black lines in Fig. 4(a)]. Here, the spontaneously-generated defects tend to decay within Rb, with Cs failing to condense into a dark-bright solitary wave and instead condensing gradually at the trap edges [Fig. 4(c)]. For quenches with large μ'_{Cs} [Fig. 4(a), green triangles], and despite the early

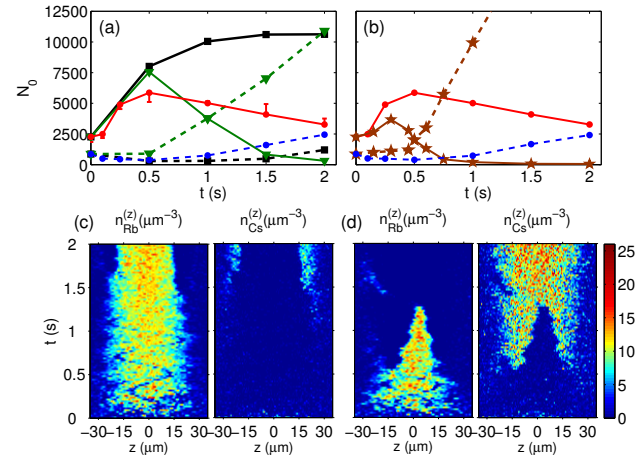


FIG. 4. (color online). Dependence of evolution on quench parameters. (a) shows condensate number evolution (Rb solid, Cs dashed) for different final chemical potentials μ'_k ; standard parameters $\mu'_{\text{Rb}} = \mu_{\text{Rb}}$, $\mu'_{\text{Cs}} = 7.34\mu_{\text{Cs}}$ (red/blue circles); $\mu'_{\text{Rb}} = 2.63\mu_{\text{Rb}}$, $\mu'_{\text{Cs}} = 7.34\mu_{\text{Cs}}$ [black squares, example c-field density evolution shown in (c)] ; $\mu'_{\text{Rb}} = \mu_{\text{Rb}}$, $\mu'_{\text{Cs}} = 11.9\mu_{\text{Cs}}$ [green triangles, example c-field density evolution shown in (d)]. Error bars in (a) for standard parameters indicate the standard deviation over 6 numerical trajectories. (b) shows condensate number evolution for different rates γ_k ; standard parameters $\gamma_{\text{Cs}} = \gamma_{\text{Rb}} = 0.263 \text{ s}^{-1}$ (red/blue circles), and $\gamma_{\text{Cs}} = 10\gamma_{\text{Rb}} = 2.63 \text{ s}^{-1}$ (brown stars).

atom number evolution remaining practically unchanged, Cs condensation rapidly outgrows that of Rb, which gradually disappears [Fig. 4(d)]. We have also investigated the effect of the growth rate on the condensate evolution (standard estimates [68] suggest that $\gamma_{\text{Cs}} \sim 10\gamma_{\text{Rb}}$), and find that increasing the ratio of $\gamma_{\text{Cs}}/\gamma_{\text{Rb}}$, for fixed chemical potentials, favours the rapid growth of Cs (after a short initial timescale of rapid Rb growth) [Fig. 4(b)].

Role of Quasi-Condensation in Pre-Quench States: Our previous simulations indicate a consistent predominance of rapid Rb growth *initially*, set by the pre-quench conditions, with long-term evolution dictated by the quench parameters. Although our initial states featured no single macroscopically-occupied state in either component, both initial states exhibited quasi-condensation, with multiple states having occupations greater than half that of the most-occupied (PO) state [≈ 10 states for Rb (largest occupation ≈ 2200), and ≈ 5 states for Cs (largest occupation ≈ 1100)]. To demonstrate the generality of our findings, we consider here (Fig. 5) the role of decreasing the initial Rb quasi-condensation, i.e. changing μ_{Rb} from > 0 [Fig. 5(c)] to ≈ 0 [Fig. 5(d)] and < 0 [Fig. 5(e)], while allowing for an initial, more pronounced, Cs quasi-condensate (through the increased $\mu_{\text{Cs}} = 2.1\hbar\omega_{\perp}^{\text{Cs}}$). Indeed, such changes imply that the initial growth becomes increasingly dominated by Cs; moreover, for conditions where Cs BEC growth dominates early on [Fig. 5(f)], we find that enhancing the final Rb chemical potential, μ'_{Rb} , can both lead to states with approximately equal Rb and Cs condensate number, or even to the generation of a quasi-stable Cs defect en-

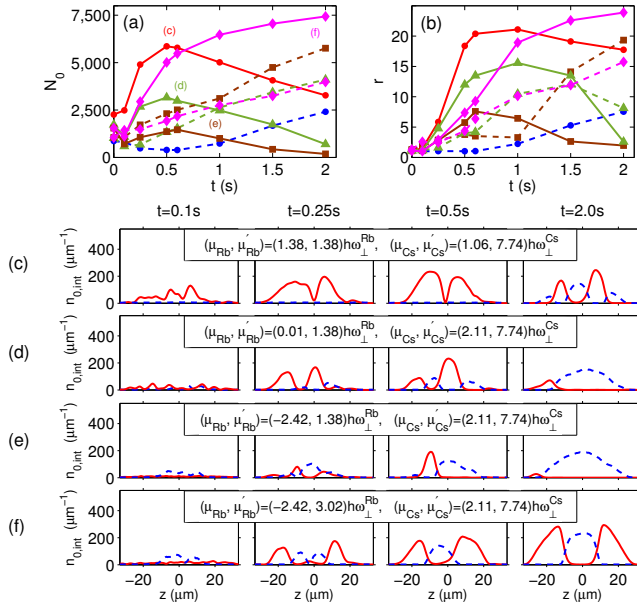


FIG. 5. (color online). Evolution of (a) condensate atom number, (b) occupation ratio r , and (c)–(f) coupled 1D integrated condensate density profiles for initial states with different amount of coherence in the Rb initial state; shown are cases with $\mu_{\text{Cs}} > 0$ and (c) $\mu_{\text{Rb}} = 1.38\hbar\omega_{\perp}^{\text{Rb}}$ (corresponding to “reference” Fig. 2 data, plotted only for ease of comparison here), (d) $\mu_{\text{Rb}} = 0.01\hbar\omega_{\perp}^{\text{Rb}}$, and (e)–(f) $\mu_{\text{Rb}} = -2.42\hbar\omega_{\perp}^{\text{Rb}}$; (f) differs from (e) only in the larger post-quench Rb chemical potential [$\mu'_{\text{Rb}} = 3.02\hbar\omega_{\perp}^{\text{Rb}}$ in (f), as opposed to $1.38\hbar\omega_{\perp}^{\text{Rb}}$ in (e)]. Note that for (d)–(f) μ_{Cs} is increased to $2.11\hbar\omega_{\perp}^{\text{Cs}}$.

abling the short-time formation and entrapment of a Rb condensate ($t = 0.25\text{s}$).

Experimental Relevance: Recent experiments have explored the emergent immiscible density profiles following the sympathetic cooling of ^{87}Rb – ^{85}Rb [41], or ^{87}Rb – ^{133}Cs [42] mixtures. Although our present work is based on a sudden quench, rather than the much smoother process of sympathetic cooling used in the experiments, we can still draw some interesting, albeit indirect, analogies: (i) both experiments sometimes found (depending on input parameters) only a single condensate present, rather than co-existence of the mixture, in qualitative agreement with the long-term evolution of our stochastic simulations; (ii) our simulations reveal long-lived metastable phase-separated profiles resembling in shape those seen in the experiment [42]; while the coupled system generally wishes to reduce its energy by minimizing the number of domains present, the large aspect ratio (more pronounced in [41]) makes such transitions energetically costly, with Ref. [41] reporting metastable states with lifetimes exceeding 1s, consistent with our above timescales; (iii) the relative timescale of condensation is important in determining the shape of the emerging profiles, as the component condensing second (typically the one with the smaller initial atom number, and so lower critical temperature) can only do so in the regions of low density of the other component [41, 42]; this explains why the most common outcome of Fig. 3 in the

probed timescales is a central Rb condensate surrounded by (the more massive) Cs (a feature which cannot be easily reproduced at equilibrium [60]). The long-term evolution will, in principle, wash out fluctuations from the formation dynamics (although in practise the timescales may be so long as to be experimentally irrelevant); indeed, the long-term outcome of Fig. 2 ($\geq 3\text{s}$) leads to the coalescence of the two decreasing phase-separated Rb peaks into a single structure surrounded by Cs. Interestingly, in a large number of simulations, this coalescence appears to occur consistently shortly after the Rb condensate number decreases to below the corresponding Cs number, providing a plausible indirect explanation for the observation of such a regime in Ref. [42].

Conclusions: We have qualitatively analysed the formation dynamics of immiscible two-component condensates following a sudden temperature quench, elucidating the importance of composite defect formation and dynamics. While our model is computationally challenging (even the coupled dissipative model, without noise, has 8 independent parameters), analysis of over 100 3D stochastic simulations has enabled us to broadly classify the quench dynamics into 3 evolution stages: initial condensation of the fastest-growing component, with dynamics mainly determined by the pre-quench state and final temperature, in which multiple defects are spontaneously formed; fluctuation-determined coarse-graining dynamics, during which defects in the prevailing component coalesce and gradually decay, potentially yielding a small number of long-lived defects; and relaxation, with long-term dynamics set by the quench parameters, during which the second component condenses in regions of low mean-field density. Importantly, a statistically non-negligible fraction ($\gtrsim 30\%$) of the cases studied exhibit a composite defect, whose spontaneous formation and subsequent evolution leads to stark shot-to-shot variations in the observable phase-separated density patterns over a broad range of experimentally relevant timescales. By varying the initial state and quench parameters, we have confirmed that both species may exhibit a defect-induced microtrap following an instantaneous quench, demonstrating the generic nature of such features.

While the prevailing composite defect in our inhomogeneous system is a dark-bright solitary wave, higher dimensional analogues are also possible, and the related “core condensation” dynamics in the context of condensed matter and high energy physics remain only partly understood even in uniform systems [30, 31]. Controlled experiments with cold atoms could help shed further light on this important problem, e.g. by statistically analysing the dynamics for different initial states and quench protocols in both box and harmonic traps.

We acknowledge funding from the UK EPSRC (Grant Nos. EP/K03250X/1, EP/K030558/1). IKL and SCG were supported by the National Science Council, Taiwan (Grant No. 100-2112-M-018-001-MY3). TPB was supported by the John Templeton Foundation via the Durham Emergence Project (<http://www.dur.ac.uk/emergence>).

[1] M. C. Cross and P. C. Hohenberg, *Rev. Mod. Phys.* **65**, 851 (1993).

[2] E. Meron, *Phys. Rep.* **218**, 1 (1992).

[3] J. D. Murray, *Mathematical biology. II, Spatial models and biomedical applications*, Interdisciplinary Applied Mathematics (Springer, 2003).

[4] H. T. C. Stoof, *Phys. Rev. Lett.* **78**, 768 (1997).

[5] Y. Kagan and B. V. Svistunov, *Phys. Rev. Lett.* **79**, 3331 (1997).

[6] D. V. Semikoz and I. I. Tkachev, *Phys. Rev. D* **55**, 489 (1997).

[7] E. Levich and V. Yakhot, *J. Phys. A* **11**, 2237 (1978).

[8] H.-J. Miesner, D. M. Stamper-Kurn, M. R. Andrews, D. S. Durfee, S. Inouye, and W. Ketterle, *Science* **279**, 1005 (1998).

[9] C. W. Gardiner, M. D. Lee, R. J. Ballagh, M. J. Davis, and P. Zoller, *Phys. Rev. Lett.* **81**, 5266 (1998).

[10] M. J. Bijlsma, E. Zaremba, and H. T. C. Stoof, *Phys. Rev. A* **62**, 063609 (2000).

[11] D. M. Stamper-Kurn, H.-J. Miesner, A. P. Chikkatur, S. Inouye, J. Stenger, and W. Ketterle, *Phys. Rev. Lett.* **81**, 2194 (1998).

[12] H. T. C. Stoof and M. J. Bijlsma, *J. Low Temp. Phys.* **124**, 431 (2001).

[13] M. Köhl, M. J. Davis, C. W. Gardiner, T. W. Hänsch, and T. Esslinger, *Phys. Rev. Lett.* **88**, 080402 (2002).

[14] N. P. Proukakis, J. Schmiedmayer, and H. T. C. Stoof, *Phys. Rev. A* **73**, 053603 (2006).

[15] M. Hugbart, J. A. Retter, A. F. Varón, P. Bouyer, A. Aspect, and M. J. Davis, *Phys. Rev. A* **75**, 011602 (2007).

[16] S. Ritter, A. Öttl, T. Donner, T. Bourdel, M. Köhl, and T. Esslinger, *Phys. Rev. Lett.* **98**, 090402 (2007).

[17] T. Donner, S. Ritter, T. Bourdel, A. Öttl, M. Köhl, and T. Esslinger, *Science* **315**, 1556 (2007).

[18] M. C. Garrett, A. Ratnapala, E. D. van Ooijen, C. J. Vale, K. Weegink, S. K. Schnelle, O. Vainio, N. R. Heckenberg, H. Rubinsztein-Dunlop, and M. J. Davis, *Phys. Rev. A* **83**, 013630 (2011).

[19] N. Navon, A. L. Gaunt, R. P. Smith, and Z. Hadzibabic, *Science* **347**, 167 (2015).

[20] S. Ronen, J. L. Bohn, L. E. Halmo, and M. Edwards, *Phys. Rev. A* **78**, 053613 (2008).

[21] E. del Valle, D. Sanvitto, A. Amo, F. P. Laussy, R. André, C. Tejedor, and L. Viña, *Phys. Rev. Lett.* **103**, 096404 (2009).

[22] G. Nardin, K. G. Lagoudakis, M. Wouters, M. Richard, A. Baas, R. André, L. S. Dang, B. Pietka, and B. Deveaud-Plédran, *Phys. Rev. Lett.* **103**, 256402 (2009).

[23] A.-W. de Leeuw, H. T. C. Stoof, and R. A. Duine, *Phys. Rev. A* **88**, 033829 (2013).

[24] A. Chiocchetta and I. Carusotto, *Phys. Rev. A* **90**, 023633 (2014).

[25] T. W. B. Kibble, *J. Phys. A* **9**, 1387 (1976).

[26] W. H. Zurek, *Nature* **317**, 505 (1985).

[27] W. Zurek, *Phys. Rep.* **276**, 177 (1996).

[28] T. Kibble and A. Srivastava, *J. Phys. Condens. Matter* **25**, 400301 (2013).

[29] A. del Campo, T. W. B. Kibble, and W. H. Zurek, *J. Phys. Condens. Matter* **25**, 404210 (2013).

[30] T. Kibble and A. Srivastava, *J. Phys. Condens. Matter* **25**, 400301 (2013).

[31] N. D. Antunes, P. Gandra, R. J. Rivers, and A. Swarup, *Phys. Rev. D* **73**, 085012 (2006).

[32] C. N. Weiler, T. W. Neely, D. R. Scherer, A. S. Bradley, M. J. Davis, and B. P. Anderson, *Nature* **455**, 948 (2008).

[33] G. Lamporesi, S. Donadello, S. Serafini, F. Dalfovo, and G. Ferrari, *Nat. Phys.* **9**, 656 (2013).

[34] S. Donadello, S. Serafini, M. Tylutki, L. P. Pitaevskii, F. Dalfovo, G. Lamporesi, and G. Ferrari, *Phys. Rev. Lett.* **113**, 065302 (2014).

[35] L. Corman, L. Chomaz, T. Bienaimé, R. Desbuquois, C. Weitenberg, S. Nascimbène, J. Dalibard, and J. Beugnon, *Phys. Rev. Lett.* **113**, 135302 (2014).

[36] W. H. Zurek, *Phys. Rev. Lett.* **102**, 105702 (2009).

[37] B. Damski and W. H. Zurek, *Phys. Rev. Lett.* **104**, 160404 (2010).

[38] E. Witkowska, P. Deuar, M. Gajda, and K. Rzazewski, *Phys. Rev. Lett.* **106**, 135301 (2011).

[39] A. del Campo, A. Retzker, and M. B. Plenio, *New J. Phys.* **13**, 083022 (2011).

[40] G. Modugno, M. Modugno, F. Riboli, G. Roati, and M. Inguscio, *Phys. Rev. Lett.* **89**, 190404 (2002).

[41] S. B. Papp, J. M. Pino, and C. E. Wieman, *Phys. Rev. Lett.* **101**, 040402 (2008).

[42] D. J. McCarron, H. W. Cho, D. L. Jenkin, M. P. Köppinger, and S. L. Cornish, *Phys. Rev. A* **84**, 011603 (2011).

[43] A. Lercher, T. Takekoshi, M. Debatin, B. Schuster, R. Rameshan, F. Ferlaino, R. Grimm, and H.-C. Nägerl, *Eur. Phys. J. D* **65**, 3 (2011).

[44] S.-W. Su, S.-C. Gou, A. Bradley, O. Fialko, and J. Brand, *Phys. Rev. Lett.* **110**, 215302 (2013).

[45] J. Sabbatini, W. H. Zurek, and M. J. Davis, *Phys. Rev. Lett.* **107**, 230402 (2011).

[46] J. Sabbatini, W. H. Zurek, and M. J. Davis, *New J. Phys.* **14**, 095030 (2012).

[47] J. Hofmann, S. S. Natu, and S. Das Sarma, *Phys. Rev. Lett.* **113**, 095702 (2014).

[48] L. E. Sadler, J. M. Higbie, S. R. Leslie, M. Vengalattore, and D. M. Stamper-Kurn, *Nature* **443**, 312 (2006).

[49] H. Saito, Y. Kawaguchi, and M. Ueda, *J. Phys. Condens. Matter* **25**, 404212 (2013).

[50] T. Świłocki, E. Witkowska, J. Dziarmaga, and M. Matuszewski, *Phys. Rev. Lett.* **110**, 045303 (2013).

[51] E. Witkowska, J. Dziarmaga, T. Świłocki, and M. Matuszewski, *Phys. Rev. B* **88**, 054508 (2013).

[52] D. M. Stamper-Kurn and M. Ueda, *Rev. Mod. Phys.* **85**, 1191 (2013).

[53] S. De, D. L. Campbell, R. M. Price, A. Putra, B. M. Anderson, and I. B. Spielman, *Phys. Rev. A* **89**, 033631 (2014).

[54] T. Busch and J. R. Anglin, *Phys. Rev. Lett.* **87**, 010401 (2001).

[55] P. Öhberg and L. Santos, *Phys. Rev. Lett.* **86**, 2918 (2001).

[56] U. Shrestha, J. Javanainen, and J. Ruostekoski, *Phys. Rev. Lett.* **103**, 190401 (2009).

[57] C. Becker, S. Stellmer, P. Soltan-Panahi, S. Dörscher, M. Baumert, E.-M. Richter, J. Kronjäger, K. Bongs, and K. Sengstock, *Nat. Phys.* **4**, 496 (2008).

[58] C. Hamner, J. J. Chang, P. Engels, and M. A. Hoefer, *Phys. Rev. Lett.* **106**, 065302 (2011).

[59] C. Hamner, Y. Zhang, J. J. Chang, C. Zhang, and P. Engels, *Phys. Rev. Lett.* **111**, 264101 (2013).

[60] R. W. Pattinson, T. P. Billam, S. A. Gardiner, D. J. McCarron, H. W. Cho, S. L. Cornish, N. G. Parker, and N. P. Proukakis, *Phys. Rev. A* **87**, 013625 (2013).

[61] M. Trippenbach, K. Gral, K. Rzazewski, B. Malomed, and Y. B. Band, *J. Phys. B* **33**, 4017 (2000).

[62] K. Kasamatsu and M. Tsubota, *Phys. Rev. A* **74**, 013617 (2006).

[63] K. Sasaki, N. Suzuki, and H. Saito, *Phys. Rev. A* **83**, 033602 (2011).

[64] V. Achilleos, D. Yan, P. G. Kevrekidis, and D. J. Frantzeskakis, *New J. Phys.* **14**, 055006 (2012).

[65] R. W. Pattinson, N. G. Parker, and N. P. Proukakis, *J. Phys. Conf. Ser.* **497**, 012029 (2014).

[66] N. G. Berloff, *Phys. Rev. Lett.* **94**, 120401 (2005).

[67] M. J. Edmonds, K. L. Lee, and N. P. Proukakis, *Phys. Rev. A* **91**, 011602 (2015).

[68] P. B. Blakie, A. S. Bradley, M. J. Davis, R. J. Ballagh, and C. W. Gardiner, *Adv. Phys.* **57**, 363 (2008).

[69] A. S. Bradley and P. B. Blakie, *Phys. Rev. A* **90**, 023631 (2014).

[70] In order to make our simulations numerically tractable, we use a plane wave basis without strict dealiasing (a procedure subtly different from Refs. [68, 79]). However, we have confirmed that our main results remain qualitatively similar when the cutoff is changed by $\sim 10\%$.

[71] Here dW_k is complex white noise defined by $\langle dW_k^*(\mathbf{x}, t) dW_j(\mathbf{x}', t) \rangle = 2\gamma_k \delta_{kj} \delta_{C;k}(\mathbf{x} - \mathbf{x}') dt$, where $\delta_{C;k}(\mathbf{x} - \mathbf{x}') = \sum_l^{E_l \leq E_{C;k}} \phi_l^*(\mathbf{x}') \phi_l(\mathbf{x})$.

[72] O. Penrose and L. Onsager, *Phys. Rev.* **104**, 576 (1956).

[73] J. Brand and W. P. Reinhardt, *Phys. Rev. A* **65**, 043612 (2002).

[74] K. J. H. Law, P. G. Kevrekidis, and L. S. Tuckerman, *Phys. Rev. Lett.* **105**, 160405 (2010).

[75] D. M. Stamper-Kurn, H.-J. Miesner, A. P. Chikkatur, S. Inouye, J. Stenger, and W. Ketterle, *Phys. Rev. Lett.* **81**, 2194 (1998).

[76] S. Coen and M. Haelterman, *Phys. Rev. Lett.* **87**, 140401 (2001).

[77] D. M. Stamper-Kurn, H.-J. Miesner, A. P. Chikkatur, S. Inouye, J. Stenger, and W. Ketterle, *Phys. Rev. Lett.* **83**, 661 (1999).

[78] S. P. Cockburn, H. E. Nistazakis, T. P. Horikis, P. G. Kevrekidis, N. P. Proukakis, and D. J. Frantzeskakis, *Phys. Rev. Lett.* **104**, 174101 (2010).

[79] P. B. Blakie, *Phys. Rev. E* **78**, 026704 (2008).